Volume 6
Number 22
21 November 2025
Pages 8195–8726

Materials Advances

rsc.li/materials-advances

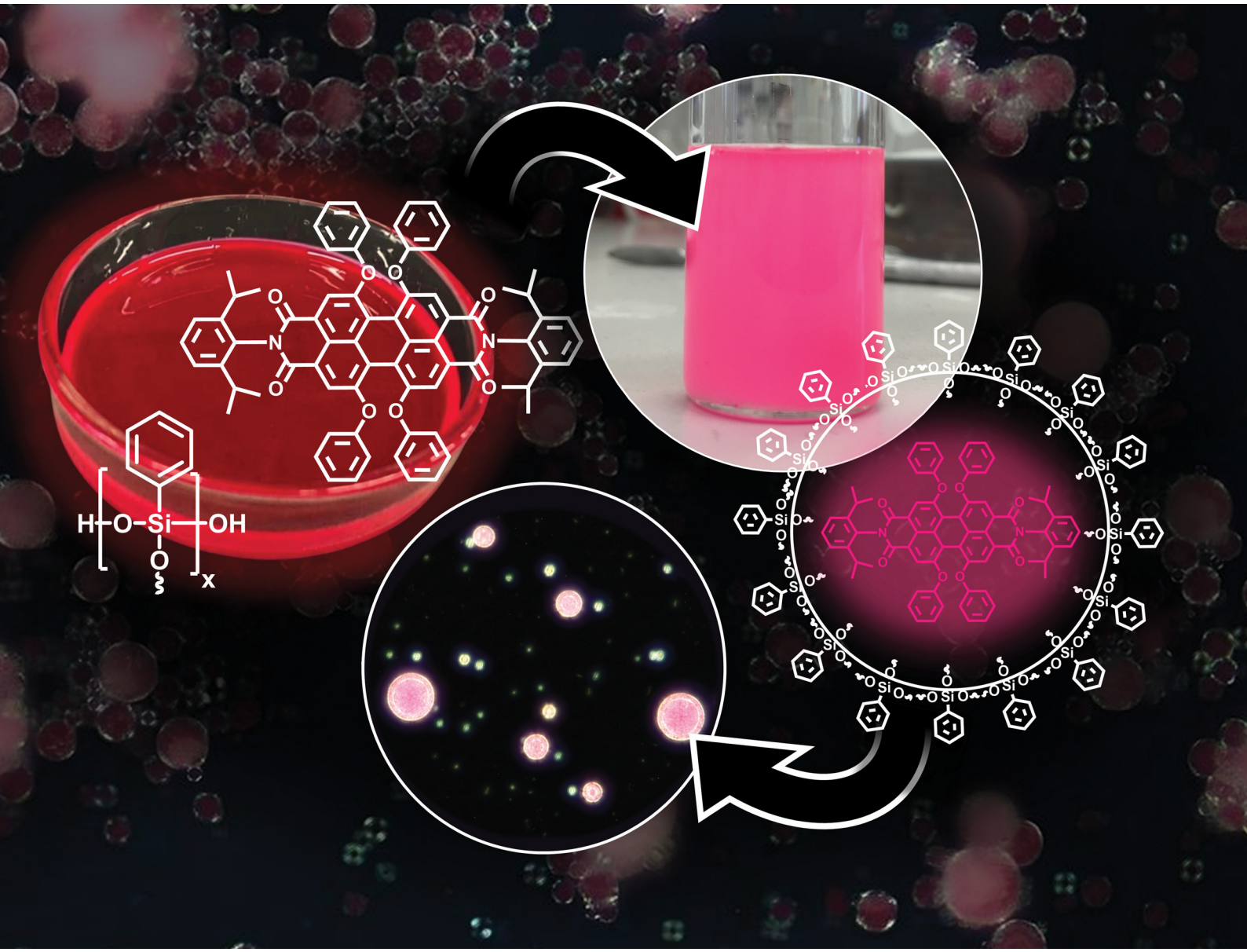

ISSN 2633-5409

ROYAL SOCIETY OF CHEMISTRY

PAPER

Guido Kickelbick *et al.*

Melt, mix, and glow: emulsion-based fabrication of polyphenylsilsesquioxane microspheres with embedded hydrophobic fluorophores

Materials Advances

ROYAL SOCIETY OF CHEMISTRY

PAPER

View Article Online
View Journal | View Issue

Cite this: *Mater. Adv.*, 2025, 6, 8379

Melt, mix, and glow: emulsion-based fabrication of polyphenylsilsesquioxane microspheres with embedded hydrophobic fluorophores

Svenja Pohl, †[a] Nils Steinbrück, †[a] Michał P. Pachnicz [a] and Guido Kickelbick *[ab]

A novel melt-emulsion strategy is presented for synthesizing polyphenylsilsesquioxane (PPSQ) microspheres embedded with hydrophobic perylene-based fluorescent dyes. The approach utilizes a low-crosslinked, thermally softenable PPSQ precursor – referred to as a "melting gel" – which incorporates polycyclic aromatic dyes such as Lumogen® F Red 305 (LG305) taking advantage of both hydrophobic compatibility and π–π interactions within the phenyl-rich matrix. Upon heating above 70 °C, the precursor forms an emulsion in boiling water containing Triton™ X-405, followed by sodium hydroxide-induced condensation to yield solid microspheres (~3 μm diameter). A subsequent thermal treatment at 200 °C enhances crosslinking, forming a condensed $PhSiO_{1.5}$ network and removing surfactant residues, thereby shifting surface polarity from hydrophilic to hydrophobic. Comprehensive characterization using NMR, FTIR, XRD, TGA, fluorescence spectroscopy, fluorescence lifetime and quantum yield analysis confirms the formation of a ladder-type silsesquioxane structure and retention of dye fluorescence. This two-step process enables efficient encapsulation of various hydrophobic dyes across a wide concentration range, offering a versatile platform for developing stable, processable luminescent materials for applications such as LED encapsulants and luminescent solar concentrators.

Received 4th August 2025,
Accepted 17th September 2025

DOI: 10.1039/d5ma00849b

rsc.li/materials-advances

Introduction

Silica- and silsesquioxane particles modified with fluorescent dyes have gained significant attention due to their versatile applications in fields such as bioimaging,[1] sensors,[2,3] light-harvesting systems[4] or light emitting diodes (LED).[5,6] Their silicon-oxide based matrix offers several advantages, including ease of surface functionalization, good biocompatibility, chemical inertness, and photochemical stability.[7–9] These properties make it an ideal host for dye molecules, providing a protective environment that minimizes both photobleaching and self-aggregation.[4,5,10] Moreover, the matrix's transparency in the visible spectrum ensures that the photophysical properties of embedded chromophores remain unaffected.[11,12]

Traditional synthesis methods for silica particles, such as the Stöber process[13] and reverse microemulsion techniques,[14] rely on sol–gel chemistry involving the acid- or base-catalyzed hydrolysis and condensation of alkoxide precursors. By employing organofunctional alkoxysilanes as precursors, organically modified silica (ORMOSIL) nanoparticles can be produced, with tunable properties based on the nature of the organics substituents attached to the monomers.[15,16] Dyes may be incorporated into these matrices either covalently or non-covalently. Covalent attachment prevents dye leaching but requires suitable functional groups on the dye that can react with the alkoxysilane precursor.[17–20] While ionic dyes are relatively easy to integrate,[21,22] nonionic, hydrophobic dyes pose a significant challenge due to their poor solubility in common solvents used in the sol–gel process like water or ethanol.

Recent efforts have explored modified Stöber processes to incorporate hydrophobic aromatic dyes into phenyl-functionalized silica particles.[4,23,24] In these cases, hydrophobic and π–π stacking interactions between the phenyl groups of the trialkoxysilane precursor and aromatic dye facilitate the physical entrapment of the fluorophores within the matrix. However, dye loading remains difficult to control and is largely dependent on the phenyl group content in the matrix.[4]

An entirely different approach for particle synthesis involves melt emulsification, a technique well-established in fields such as food technology,[25] pharmaceuticals,[26] and additive manufacturing.[27] This method utilizes thermoplastic materials that are melted and emulsified in a continuous phase with

[a] *Inorganic Solid-State Chemistry, Saarland University, Campus, Building C4.1, 66123 Saarbrücken, Germany. E-mail: guido.kickelbick@uni-saarland.de*
[b] *Saarene, Saarland Center for Energy Materials and Sustainability, 66123 Saarbrücken, Germany*
† These authors contributed equally to this work.

surfactants under shear, forming droplets that solidify upon cooling into spherical particles. Despite its versatility, this approach has not been applied to silica-based systems, primarily due to the absence of thermoplastic materials with a Si–O–Si backbone.

A promising class of materials that meets the requirements for melt-emulsion processing is the so-called melting gel – a silica-based gel that is rigid and glass-like at room temperature but softens upon heating to approximately 100 °C. Further heating above 130 °C induces irreversible thermal curing.[28,29] These materials are known for their high thermal stability,[30] low gas permeability,[31] and broad-range optical transparency.[32,33] Most melting gels are functionalized with phenyl groups, which not only contribute to their thermal and optical properties but also enable non-covalent incorporation of aromatic, hydrophobic dyes such as perylene diimides. These dyes are particularly attractive for applications in luminescent solar concentrators (LSCs) and LED technologies.[34–36]

In this study, we report the synthesis of a polyphenylsilsesquioxane (PPSQ) melting gel into which various perylene-based dyes (Lumogen® F Red 305 (LG305), Oracet® FL Pink 285, Oracet® FL Orange 240) were incorporated during synthesis. This precursor gel was used to form fluorescent microspheres *via* a modified two-step melt emulsion method. In this process, the dye containing softenable gel formed an emulsion in boiling aqueous surfactant solution, which was subsequently solidified by the addition of NaOH as a basic condensation catalyst.

The successful encapsulation of the dyes was confirmed by fluorescence spectroscopy and fluorescence lifetime analysis and the effect of Lumogen® F Red 305 concentration on quantum yield was investigated. The structure of the precursor gel, as well as structural changes occurring during particle formation, were analyzed using various spectroscopic and thermal methods, as well as powder X-ray diffraction (PXRD).

Encapsulation within the PPSQ matrix not only protects the embedded fluorophores from environmental degradation but also facilitates their integration into secondary matrices, such as elastomeric materials, for use in bulk optical applications.

Experimental

Materials

Phenyltrimethoxysilane (97%, abcr GmbH, Germany), polyoxyethylene(40)isooctylphenylether solution (Triton™ X-405, 70% in water, Sigma-Aldrich/Merck KGaA, Germany), hydrochloric acid (Bernd Kraft GmbH, Germany) and sodium hydroxide (85%, Grüssing GmbH Analytica, Germany) were used as received. The commercially available, curable OE6630 polysiloxane resin (Dow, Dow Corning Inc., USA) and the perylene dyes Lumogen® F Red 305 (LG305, BASF, Germany), Oracet® FL Orange 240 (SunChemical, Germany) and Oracet® FL Pink 285 (SunChemical, Germany) were also used as received without any further purification. The hydrochloric acid was diluted with demineralized water (pH = 2.5). Sodium hydroxide was dissolved in demineralized water (3 mol l^{-1}). NMR characterization of key reactants, melting gels, and microspheres is provided in (Fig. S1–S8).

Instrumentation

Solution nuclear magnetic resonance (NMR) spectra were recorded on an Avance III 300 MHz spectrometer and an Avance III HD 400 MHz spectrometer (Bruker, Billerica, USA) with 300.13/400.13 MHz for ^{1}H NMR spectra, 75.47/100.61 MHz for ^{13}C NMR spectra and 59.63/79.49 MHz for ^{29}Si NMR spectra. NMR samples were prepared in $CDCl_3$ and D_2O. Spectra were analyzed using MestReNova.[37] Single-pulse (SP) magic angle spinning (MAS) NMR spectra were recorded on an Avance III HD – Ascend 400WB spectrometer (Bruker, Billerica, USA) using 4 mm inner diameter ZrO_2 rotors with 13 kHz rotation frequency. The resonance frequencies were 79.53 MHz for ^{29}Si NMR spectra and 100.65 MHz for ^{13}C NMR spectra. The measurements were performed with a relaxation of 20 s. Adamantane was used for ^{13}C NMR and octakis(trimethylsiloxy)silsesquioxane for ^{29}Si NMR as external standard. Peaks of ^{29}Si CP-MAS spectra were deconvoluted and integrated with a Lorentzian-Gaussian fit using MestReNova.[37] For the visualization of sub millimeter structures an Axioskop 50 transmitted light/fluorescence microscope (Carl Zeiss Microscopy GmbH, Germany) with an AxioCam MRc (1388 × 1040 pixel) was used. The particles were counted with the help of the ImageJ software (version 1.53 k).[38] Attenuated total reflectance Fourier transform infrared (ATR-FTIR) spectra were recorded on a Vertex 70 spectrometer (Bruker Optics, Billerica, USA) in total reflectance mode from 450–4500 cm^{-1} with a resolution of 4 cm^{-1} and 16 scans. Thermogravimetric analysis-Fourier transform infrared spectroscopy (TG-FTIR) was performed using a Vertex 70 spectrometer (Bruker Optics, Ettlingen, Germany) coupled to a TG F1 Iris (NETZSCH-Gerätebau GmbH, Selb, Germany). Each FTIR spectrum was performed in the wavenumber range 550–4500 cm^{-1} and by averaging 16 scans with a spectral resolution of 4 cm^{-1}. The measurements were carried out at 20 K min^{-1} heating rate in the temperature range between 30 and 1000 °C under synthetic air flow (40 mL min^{-1}, N_2/O_2 75%/25%). Fluorescence spectroscopy of particles was performed applying a FluoroMax 4 Spectrofluorometer (Horiba Scientific, Kyoto, Japan) as solid in quartz glass tubes. Absolute photoluminescence quantum yields were measured in a Quantaurus C11347-11 integration sphere setup (Hamamatsu Photonics, Hamamatsu, Japan) with a xenon high-pressure lamp and a multichannel analyzer. Fluorescence lifetime measurements were performed on the samples in the solid state using time-correlated single-photon counting (TCSPC) under magic angle conditions. A pulsed laser (λ_{exc} = 490 nm, FemtoFiber pro TVIS, Toptica Photonics, Gräfelfing, Germany, 80 MHz) served as excitation source, passed through a 470/40 bandpass clean-up filter. For detection, a photocounting detector (PDM series, Micro Photon Devices, Bolzano, Italy), a photocounting device (Pico Harp 300, PicoQuant, Berlin, Germany), and a 685/70 bandpass filter were used. An instrumental response function (IRF) was recorded with a diluted colloidal silica solution (LUDOX TM-50, Sigma-Aldrich, St. Louis, MO, USA). Data analysis was carried out with commercial software

SymPhoTime.[39] Powder X-ray diffraction (PXRD) patterns of the pulverized samples were recorded at room temperature on a D8-A25-Advance diffractometer (Bruker-AXS, Karlsruhe, Germany) in Bragg–Brentano θ–θ-geometry (goniometer radius 280 mm) with non-monochromatic Cu K_α radiation (λ = 154.0596 pm). A 12 μm Ni foil working as K_β filter and a variable divergence slit were mounted at the primary beam side. A Lynxeye detector with 192 channels and a variable anti-scatter slit in front of it was used at the secondary beam side. Experiments were carried out in a 2θ range of 3 to 40° with a step size of 0.013° and a total scan time of 1 h. The recorded data was evaluated using the TOPAS 5.0 software.[40] UV-VIS measurements were performed on a Lambda 750 instrument (PerkinElmer Inc., Shelton, USA) equipped with a 100 mm integration sphere with a 2 nm increment and 0.2 s integration time. Transmission spectra of the composites, cured in aluminum frames, were recorded from 300 to 800 nm. Scanning electron microscope (SEM) images were obtained using a JEOL JSM-7000 F microscope (JEOL, Freising, Germany) operating at 20 kV with a working distance of 10 mm. The SEM samples were prepared by placing a small amount of the particles on a specimen stub covered with a carbon adhesive foil followed by deposition of a gold layer (JEOL JFC-1300 auto fine coater, 30 mA, 40 s) to avoid charging effects. The complex viscosity was determined applying a MCR-302 rheometer with a CTD-450 convection heating system (Anton Paar GmbH, Graz, Austria) in the oscillatory mode using parallel-plate geometry with an upper diameter of 25 mm, an amplitude of 1% and a frequency of 1 Hz. During the measurement the temperature was lowered from 100 °C to 55 °C with the rate of 2 K min^{-1}.

Preparation

Synthesis of precursor melting gel (MG). Following a reported procedure,[41] phenyltrimethoxysilane (7 g, 35.30 mmol) and aqueous hydrochloric acid (pH = 2.5, 0.95 g, 52.95 mmol, 1.5 eq.) were stirred in a sealed vial (45 °C, 8 h). The solution was transferred into a beaker (100 mL) and a certain amount of LG305 (Oracet® FL Orange 240 or Oracet® FL Pink 285) was added (5.15 mg, n(LG305) = 5.3 μmol). The mixture was stirred until gelation was completed (25 °C, 18 h), visible by a significant increase in viscosity. The beaker was transferred into a vacuum oven to interrupt reactions by removing water, hydrochloric acid and methanol in two steps (30 mbar, 70 °C, 24 h; 110 °C, 24 h). The viscous and flowable red material was cooled to room temperature to obtain the solid PPSQ precursor melting gel (4.48 g, 1150 ppm dye). The material softens reversible at temperature >70 °C. At temperatures >130 °C it consolidates irreversibly. The unconsolidated material containing the dye LG305 was denoted with MG LG305. The consolidated material (200 °C, 24 h) was denoted with $MG_{cons.}$ LG305.

For concentration-dependent quantum yield measurements, additional MGs containing 26 000 ppm, 10 600 ppm, 4350 ppm, 2450 ppm and 220 ppm of LG305 were prepared by simply adjusting the amount of dye added during synthesis. The exact sample weights and calculated dye concentrations are provided in (Table S1).

Table 1 Variation of stirring rate, stirring time and dispersion method for the synthesis of MGP LG305

Sample	Stirring rate [rpm]	Stirring time
MGP-1	500	1 h
MGP-2	500	2 h
MGP-3	800	1 h
MGP-US	500	10 min
	Only ultra-sonic (150 W)	2 min
MGP-UT	500	10 min
	10 000 (disperser)	2 min

Synthesis of melting gel microspheres (MGP). Polyoxyethylene(40)isooctylphenylether solution (90 mg, Triton™ X-405, 70 wt% in water (~0.356 mmol g^{-1})) was added to water (14 mL, 0.77 mol) and stirred at 500 rpm at 100 °C. The precursor melting gel (100 mg) was then added to the hot solution, forming an emulsion upon softening. Stirring was continued at a 800 rpm for 1 h at 100 °C. A sodium hydroxide solution (1 mL, 3 mol L^{-1}) was subsequently added to the emulsion, followed by further stirring at 500 rpm for 1 h at 100 °C. The emulsion was then cooled in an ice bath. The resulting melting gel microspheres were isolated by centrifugation, washed four times with water, and dried in a compartment drier under reduced pressure (80 °C, 5 mbar). The product obtained from MG LG305 was denoted as MGP LG305.

To investigate the influence of varying mechanical energy input on particle morphology, five experiments were conducted using different stirring procedures (Table 1), employing MG LG305 (1150 ppm). Different stirring rates and durations were tested, along with the effect of high-energy processes, by applying an ultrasonic probe (US) (150 W) and an Ultra-Turrax™ disperser (UT) (10 000 rpm) after an initial stirring at 500 rpm for 10 min at 100 °C. The specified stirring rates and durations refer to the experimental steps prior to the addition of sodium hydroxide. After the base was added, all samples were stirred at 500 rpm for 1 h at 100 °C. Particle size and distribution were determined by measuring and counting particles from microscopy images.

Post-curing. For further investigations of temperature-induced changes in structure or heat stability, the MGP LG305 microspheres were additionally heat treated in a post-curing process (200 °C, 24 h). The obtained tempered particles were denoted with MGP-T LG305.

Particle integration in polyphenylmethylsiloxane resin. MGP-T microspheres (1 wt% of MGP-T (1150 ppm dye)) were added to the polyphenylmethylsiloxane resin Dow Corning OE6630 (Dow). The two Dow components, A and B, were premixed according to the manufacturer's specifications (1/4). The particles were then incorporated into this matrix, and gas was removed under reduced pressure (4 mbar, >30 min). The degassed mixture was cast into aluminum frames (8 × 2 mm) and cured for 2 h at 150 °C.

Results and discussion

Synthesis and characterization of the dye-doped precursor

The dye-doped precursor melting gel was synthesized *via* an acid-catalyzed polycondensation reaction of phenyltrimethoxysilane,

forming partially crosslinked structures.[41,42] During the gelation step a perylene-based dye (Lumogen® F 305 Red, Oracet® FL Orange 240 or Oracet® FL Pink 285) was added (Fig. 1). At this stage, oligomeric phenylsilsesquioxane and methanol generated from hydrolysis and partial condensation are present, providing a medium in which the dye is soluble. This enables homogeneous incorporation into the network despite its insolubility in water. In the following, we will concentrate on the characterization of the material containing Lumogen® F 305 Red (MG LG305, 1150 ppm dye).

The resulting material is a rigid, transparent, red-colored solid, soluble in organic solvents and thermally softenable above 70 °C. Rheological measurements (Fig. S10) confirm its softening behavior. Upon thermal treatment above 130 °C, irreversible curing occurs, yielding $MG_{cons.}$ LG305, which is insoluble and no longer softenable. The structural properties of both the precursor and the cured precursor, excluding the dye, have been thoroughly examined in a previous study.[41]

FTIR spectroscopy of MG LG305 reveals the expected vibration bands of the PPSQ network, including broad ν(Si–O–Si) vibrations between 1000 and 1150 cm^{-1} and phenyl group associated signals at 3080–3010 ($(C–H)_{ring}$), 1595 and 1430 cm^{-1} ($\nu(C–C)_{ring}$) and 1130 cm^{-1} ($\nu(Si–C)_{ring}$). Additional vibration bands at 3380 ($\nu(O–H)_{associated}$), 3620 ($\nu(O–H)_{isolated}$), 910 (ν(Si–OH)), 2940–2840 ($\nu(C–H(O–CH_3))$), 1090 and 806 cm^{-1} ($\nu(Si–O–CH_3)$) indicate the presence of residual hydroxy and methoxy groups (Fig. 2).[43–45]

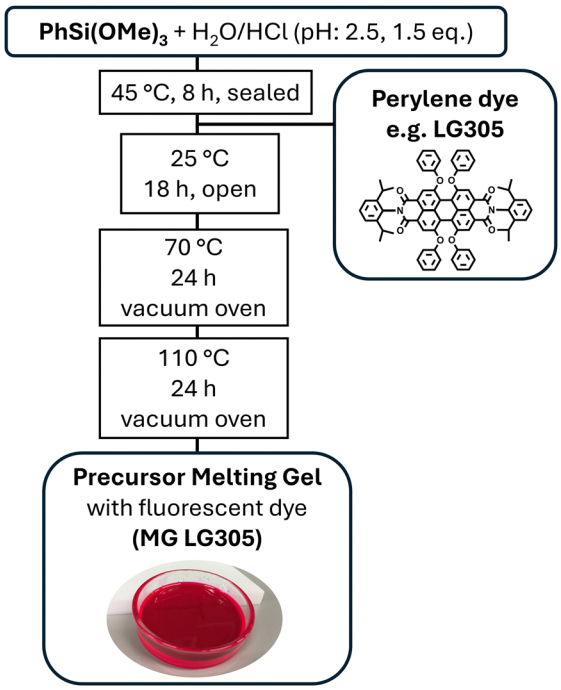

Fig. 1 Synthesis procedure for the Lumogen® F 305 Red (LG305) containing polyphenylsilsesquioxane precursor melting gel (MG LG305). The amount of monomer and dye loading can be adjusted; in this study, samples with dye concentrations between 220 and 26 000 ppm were prepared. Alternatively, other hydrophobic dyes can be incorporated using the same approach.

^{1}H and ^{13}C NMR spectra confirm the presence of phenyl and methoxy groups, with phenyl proton signals between 7.84–6.65 ppm and methoxy proton signals at 3.76–2.86 ppm. The estimated remaining methoxy group content is around 10% (Fig. S4). The corresponding carbon chemical shifts appear at 134.35–127.83 ppm (phenyl) and 50.65 ppm (OCH_3) (Fig. 3(a)). Due to the low dye concentration (1150 ppm) in the sample investigated, signals from the integrated dye are barely visible in both the IR and NMR spectra.

^{29}Si NMR spectra indicate a partially crosslinked structure, predominantly composed of T^2 (−71.6 ppm) and T^3 (−79.5 ppm) units, where T refers to a silicon atom bonded to one carbon atom and three oxygen atoms, while the superscript denotes the number of siloxane bonds (Si–O–Si) per unit. The percentage share of T^2 and T^3 is 53% and 40%, as determined by deconvolution of ^{29}Si SP-MAS NMR spectra (Fig. 3(b) and Fig. S5). The low degree of condensation (DC) of 78%, along with residual alkoxy and hydroxy groups causes flexibility of the polymer chains at elevated temperatures and explains reversible softening and solubility.[41]

Thermal treatment of the precursor at 200 °C induces further condensation of residual OH and OCH_3 groups, resulting in irreversible consolidation. This is evidenced by a TGA mass loss of 4% starting at about 200 °C. The evolved gas analysis by FTIR at these temperatures shows characteristic vibrations of the condensation by-products, methanol and water (Fig. S11). Following this consolidation step, degradation of the organic groups and the polymer network begins only at 500 °C, demonstrating the material's high thermal stability. The FTIR spectrum of the cured material shows a reduction in OH-associated bands at 3380 cm^{-1} (Fig. 2), while ^{29}Si SP-MAS NMR indicates an increase in T^3 units and a decrease in T^2 and T^1 species (Fig. 3(b)) consistent with further crosslinking. However, the presence of residual OCH_3 groups detected in ^{13}C SP-MAS NMR, along with a degree of condensation of 83%, and the persistence of isolated OH group, observed in FTIR spectra at 3620 cm^{-1}, suggest incomplete crosslinking. This partial crosslinking of phenyltrialkoxysilanes was already reported for silsesquioxane-based particles and can be explained by the bulky phenyl substituents that sterically hinder the formation of dense T^3 networks.[15,46,47] Nevertheless, the crosslinking is sufficient to eliminate chain mobility, rendering the material insoluble and thermally stable.

PXRD and FTIR spectroscopy provide more detailed insights into the structure of silsesquioxanes, which typically include cage, open-cage, and ladder structures, as well as random silsesquioxanes or mixtures thereof.[48] PXRD analysis reveals two broad amorphous peaks, indicative of ladder-like structural motifs (Fig. 4). The first reflection (d_1) corresponds to interchain distances modulated by phenyl groups, while the second (d_2) relates to Si–O–Si spacing.[49–51]

Thermal curing leads to a shift of $2\theta_{d_1}$ to lower values (larger chain-to-chain distance), an increase in the $2\theta_{d_1}/2\theta_{d_2}$ intensity ratio, as well as a sharpening of $2\theta_{d_1}$ reflection (reduction in full width at half maximum) (Table S2). These changes indicate enhanced structural order and an increase in ladder-like content in the $MG_{cons.}$ LG305.[52,53]

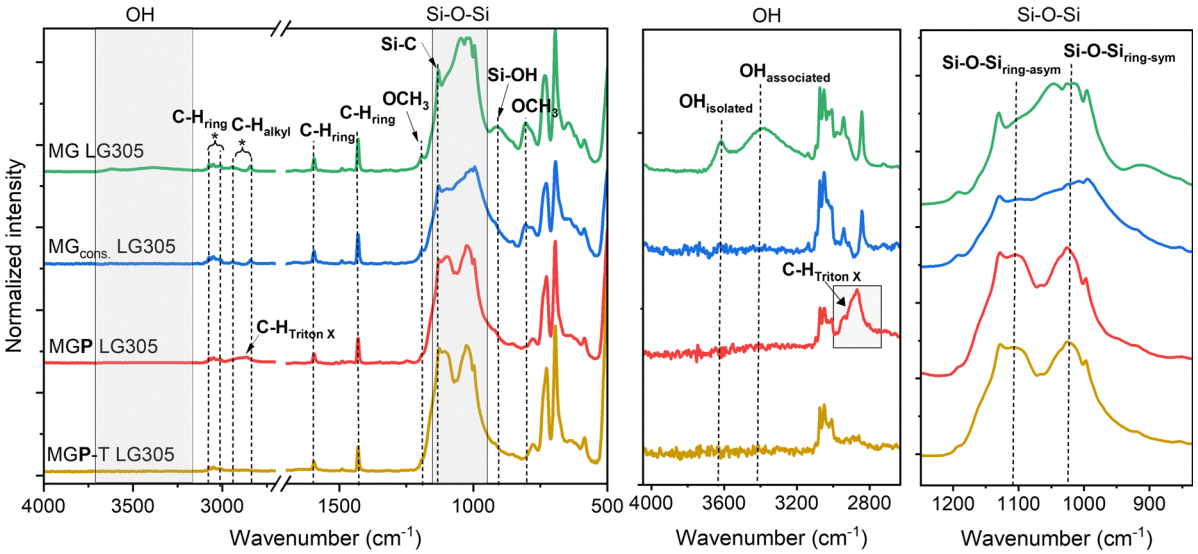

Fig. 2 FTIR spectra of MG LG305, $MG_{cons.}$ LG305, MGP LG305 and MGP-T LG305, showing the full spectrum and a magnified view of the OH-group region and the Si–O–Si vibration region with assignment of the most important vibrations.

FTIR spectra support this interpretation, showing a moderate splitting of the Si–O–Si stretching vibrations at $\nu(\text{Si–O–Si})_{\text{ring-asym}}$ = 1106 cm^{-1} and $\nu(\text{Si–O–Si})_{\text{ring-sym}}$ = 1023 cm^{-1}, characteristic of ladder-like architectures.[54,55] However, the intensity of $\nu(\text{Si–O–Si})_{\text{ring-asym}}$ coming from highly symmetrical $(\text{Si–O})_4$ ring subunits is significantly lower than that observed for phenyl ladders reported in the literature.[50,56,57] Furthermore the Si–O–Si region is quite unstructured, indicating a high number of defects caused by residual hydroxy and methoxy groups, random structural units with various silsesquioxane motifs, such as small rings or open and closed cages.[41]

Overall, the integration of LG305 does not significantly affect the hydrolysis or condensation behavior of phenyltrimethoxysilane and the final structure of the precursor gel, due to the low dye concentration. At the loading of 1150 ppm used in the material investigated here, the dye is barely detectable by

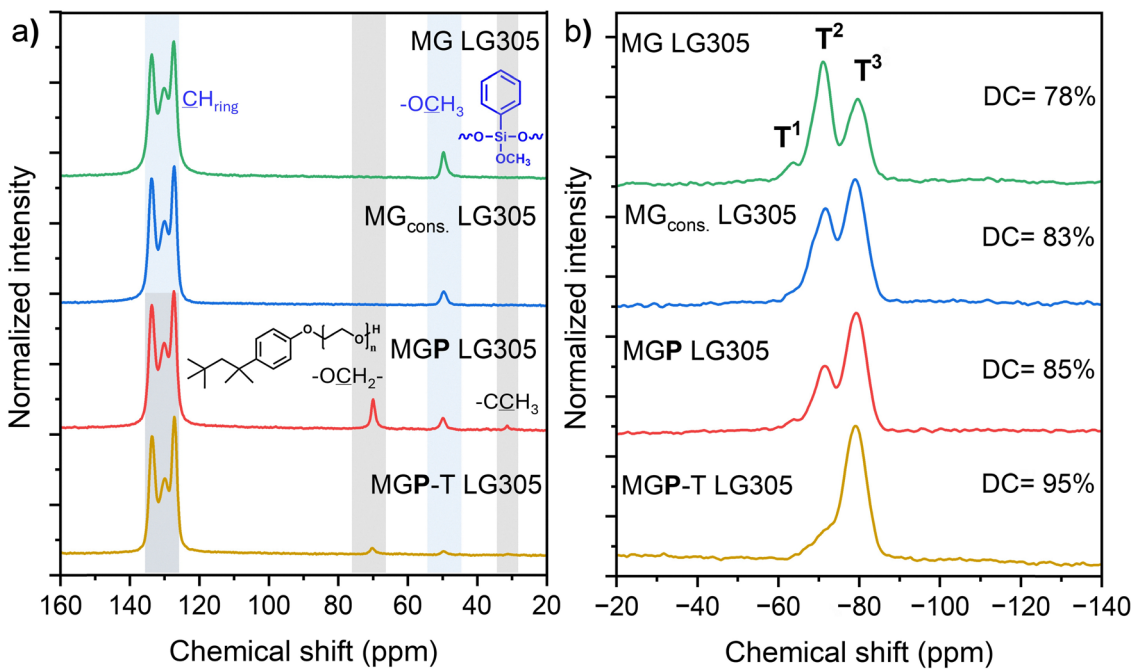

Fig. 3 (a) ^{13}C SP-MAS NMR spectra of MG LG305, $MG_{cons.}$ LG305, MGP LG305 and MGP-T LG305, illustrating the removal of the surfactant and further condensation of the microsphere structure, (b) ^{29}Si SP-MAS NMR spectra of MG LG305, $MG_{cons.}$ LG305, MGP LG305 and MGP-T LG305, showing the changes in T units and the degree of condensation (DC), calculated from deconvoluted ^{29}Si SP-MAS NMR spectra according to the formula: DC (%) = (T^3 (%)·3 + T^2 (%)·2 + T^1 (%))/3.

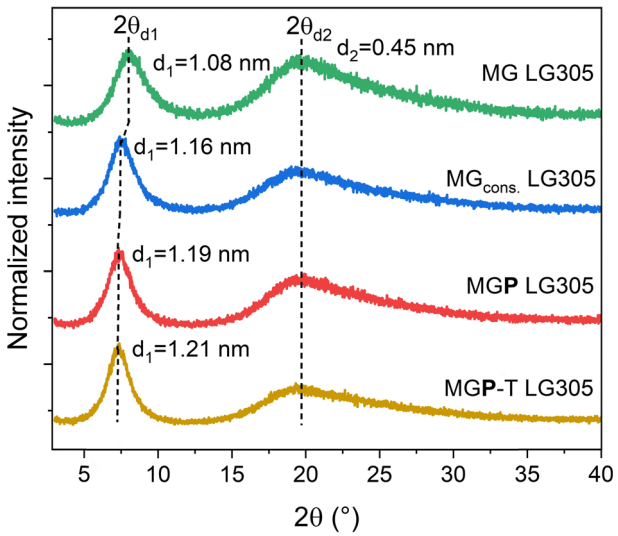

Fig. 4 Powder XRD patterns of MG LG305, $MG_{cons.}$ LG305, MGP LG305 and MGP-T LG305 with marked positions of $2\theta_{d_1}$ and $2\theta_{d_2}$ and corresponding d_1 and d_2 values.

NMR and IR spectroscopy. Only at an increased concentration of over 2000 ppm do peaks appear in the NMR spectra that can be attributed to LG305 (Fig. S9).

Formation of microspheres *via* melt emulsion

For the subsequent formation of microspheres, MG LG305 was added to a boiling aqueous solution of the nonionic surfactant Triton™ X-405 (Fig. 5). Upon heating, the material softened, and continuous stirring led to the formation of a hot emulsion in which the surfactant stabilized the molten droplets, preserving their spherical morphology and controlling particle size. In the absence of surfactant, particle formation is not driven by controlled dispersion but rather by mechanical fragmentation, resulting in angular, irregularly shaped particles (Fig. S12).

The hydrophobic perylene-based dye LG305 remained confined within the organic phase, preventing leaching into the aqueous medium. Subsequent addition of NaOH initiated base-catalyzed hydrolysis and condensation of residual hydroxy and methoxy groups at the droplet surface, chemically consolidating the microspheres and preserving their shape. The resulting particles (MGP LG305) were isolated by centrifugation.

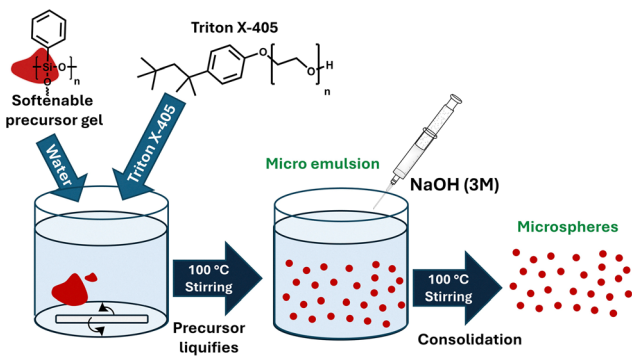

Fig. 5 Schematic workflow for the preparation of PPSQ microspheres.

Due to light scattering effects, the color of the material changed from red to pinkish (Fig. 6(a)).

Microscopic analysis reveals spherical particles within the micrometer range (Fig. 6(b)). SEM measurements confirm the spherical morphology of the particles, but also show the presence of cavities within the spheres that are larger than ≈5 μm in diameter (Fig. 6(c)). These holes can be explained by the formation of water and methanol as by-products of the base-catalyzed polycondensation reaction. As these volatile compounds evaporate, gas bubbles become trapped within the partially solidified microspheres. Since the material can no longer soften at this stage, the cavities remain open and persist within the particle structure. Consistently, similar voids are also observed in control samples prepared without surfactant (Fig. S12b), indicating that outgassing of condensation by-products is the main origin of this morphology, while the surfactant appears to have little or no direct influence on cavity formation.

Notably, such hollow features are absent in smaller microspheres <5 μm (Fig. 6(d)).

The obtained microspheres are completely insoluble in water or ethanol but exhibit swelling and partial solubility in acetone or chloroform, leading to the degradation of the particulate structure and leaching of the dye (Fig. S13 and S14). In hydrophilic

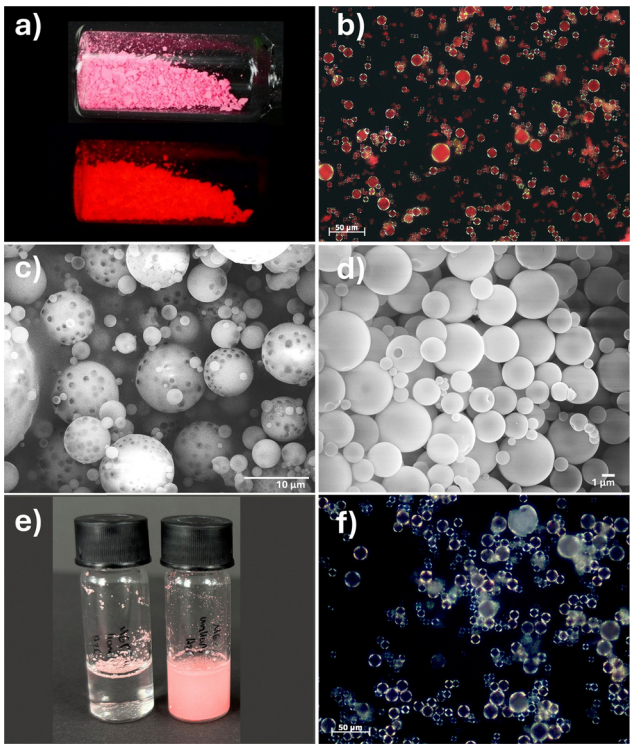

Fig. 6 (a) Image of MGP LG305 under natural light and showing red fluorescence under LED light (λ = 450 nm), (b) microscopy image of MGP LG305, dispersed in EtOH, (c) SEM image of MGP LG305 at 2500× magnification, (d) SEM image of MGP LG305 at 10 000× magnification, showing a region with sub-5 μm particle sizes, (e) image of isolated microspheres, dispersed in water, left MGP-T LG305 and right MGP LG305, (f) microscopy image of MGP-T LG305 after dispersion in acetone for 30 minutes.

solvents, the particles remain dispersible due to the residual surfactant coating from the synthesis, which imparts a hydrophilic surface to the spheres (Fig. 6(e)).

For a more comprehensive characterization of the materials structure, ^{29}Si and ^{13}C SP-MAS NMR, PXRD, FTIR spectroscopy, and thermal analysis were performed in comparison with both the precursor MG LG305 and the consolidated precursor material $MG_{cons.}$ LG305.

FTIR spectroscopy confirmed the presence of Triton™ X-405 in MGP LG305 *via* the C–H vibration at 2873 cm^{-1} in the FTIR spectrum (Fig. 2). The ^{13}C MAS-NMR spectrum (Fig. 3(a)) showed characteristic signals of both the surfactant and the PPSQ matrix. The aromatic carbons appear at 133, 130, 127 ppm (C–H (phenoxy/phenyl)) and additional signals at 70 (O–$\underline{C}H_2$) and 31 ppm (C–$\underline{C}H_3$) can be attributed to Triton™ X-405. A peak at 50 ppm indicated residual methoxy groups of the T^2 units, suggesting that the base-induced condensation also results in a partially crosslinked structure, similar to that of the $MG_{cons.}$ LG305. This result is further supported by ^{29}Si SP-MAS NMR data. In the NMR spectrum of MGP LG305, T^2 and T^3 units are observed at −71 and −79 ppm (Fig. 3(b)). The calculated percentage of T^3 units is 55%, and the DC is 85%.

Although the crosslinking of the MGP LG305 is not significantly different from that of the $MG_{cons.}$ LG305, changes in microstructure are evident in the Si–O–Si vibrational range of the FTIR spectra. The relative intensity of $\nu(\text{Si–O–Si})_{\text{ring-asym}}$ absorption band at 1106 cm^{-1} increases markedly compared to $\nu(\text{Si–O–Si})_{\text{ring-sym}}$ upon base treatment (Fig. 2). This shift indicates the formation of highly symmetrical $(SiO)_4$ subunits, suggesting a pronounced increase in ladder-type segments.[55] PXRD measurements confirm this observation, showing a further increase in the d_1 value (Fig. 4) and a narrowing of the $2\theta_{d_1}$ reflection, both of which support the higher degree of ordering within the PPSQ network.[52,53] These findings imply that NaOH-induced consolidation in an excess of water promotes rearrangement within the precursor material, yielding a more ordered architecture than thermal curing alone. It is expected that the presence of water as the reaction medium increases the number of hydrolyzed groups, facilitating hydrogen bonding and alignment of polymer chains.[58] At the same time, the basic catalyst accelerates the condensation within the preorganized regions formed by hydrogen bonding, thereby enhancing the degree of condensation within the network.[59]

The solubility and softenability of MGP LG305 are comparable to those of the consolidated precursor material. The increase in crosslinking due to the addition of basic catalyst results in a rigid structure, preventing softening and ensuring that the spherical morphology remains stable even at high temperatures. However, the incomplete crosslinking (DC = 85%) allows the particles to swell in moderately polar solvents (*e.g.* acetone, dichloromethane (DCM), toluene, dimethyl sulfoxide (DMSO)), resulting in the loss of their spherical structure and leaching of the dye (Fig. S13 and S14).

In conclusion, the thermoplastic properties of the MG LG305 facilitate the preparation of micrometer-sized spheres *via* melt emulsion, which are coated with the surfactant Triton™ X-405. When NaOH is used as a catalyst, the particles become non-softenable and maintain their spherical shape even at elevated temperatures. The particle morphology is size-dependent: larger microspheres exhibit internal cavities, while smaller ones appear uniform and compact. The treatment conditions of the precursor gel (NaOH and water) promote the formation of a more ordered PPSQ architecture with a ladder-like structure.

Thermal crosslinking of microspheres

In a subsequent thermal treatment step, the particles were heated to 200 °C for 24 hours. During this process, no softening of the particles was observed, allowing the spherical morphology to be preserved (Fig. S16). However, increasing the temperature to 200 °C leads to the removal of the surfactant from the surface, as confirmed by the TGA of MGP LG305 (Fig. 7(a)). A mass loss of 8% was detected, beginning at 230 °C. This mass loss can be assigned to the removal of Triton™ X-405 by TG-FTIR spectroscopy, including an oxidation in the hydrophilic chain and a decomposition of the surfactant under air (Fig. 7(a) and (b)).[60] In the TGA of the tempered particles, the surfactant is no longer detectable (Fig. 7(a) and (c)).

The release of Triton™ X-405 is also evident in the ^{13}C MAS NMR spectrum, where a significant decrease in the signal at 70 ppm (Fig. 3(a)) is observed. Additionally, FTIR spectroscopy confirms this removal through the disappearance of C–H vibrations between 2800 and 2900 cm^{-1} (Fig. 2). The decomposition of the surfactant on the surface of the microspheres results in a more hydrophobic surface, whereby a dispersion of the particles in hydrophilic solvents was no longer possible (Fig. 6(e)). Simultaneously, the microsphere structure undergoes further crosslinking. In the ^{13}C SP-MAS NMR spectrum, the chemical shift of the methoxy groups nearly disappears, and the ^{29}Si SP-MAS NMR spectrum shows a predominant T^3 signal at −79 ppm, with a degree of condensation of 95%, indicating the formation of a highly crosslinked $PhSiO_{1.5}$ network (Fig. 3). The significant increase in crosslinking upon NaOH treatment at elevated temperatures has also been reported by other groups.[61,62] It reveals that the thermal consolidation process of the microspheres differs from that of the precursor, where a significant amount of T^2 units remains afterwards. The increased DC and the reduction of defects in the form of OH and OCH_3 groups are also reflected in the XRD analysis by a further shift of the d_1 value to larger interplanar distances and a narrowing of the $2\theta_{d_1}$ diffraction peak (Fig. 4 and Table S2).

The results indicate a direct influence of sodium hydroxide pretreatment on the subsequent structure formation, as discussed earlier in the structural characterization of untempered MGP LG305. In the postulated ladder-like arrangement, the phenyl groups exert less steric hindrance on the nucleophilic attack of Si–OR groups, enabling almost complete condensation, as is typical for silsesquioxanes with a ladder architecture.[50,57,63]

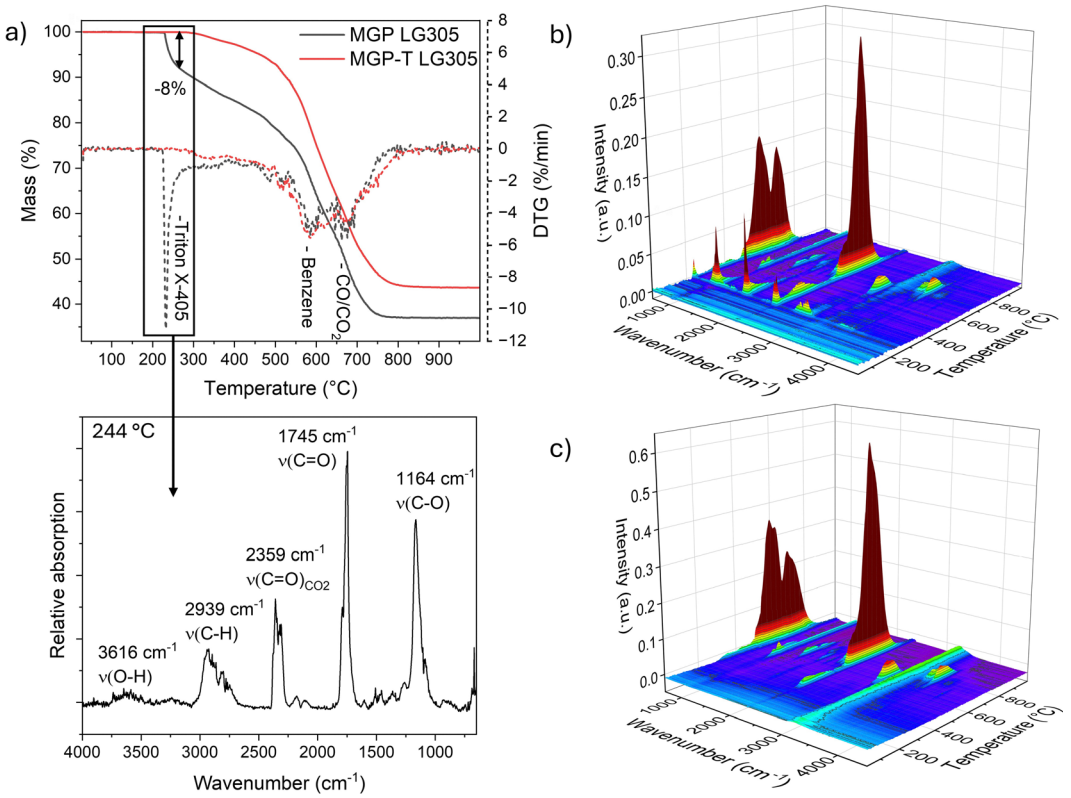

Fig. 7 (a) TGA of MGP LG305 and MGP-T LG305, along with FTIR spectrum of the gases released at the first degradation step at 244 °C for MGP LG305, (b) 3D TGA-FTIR spectrum of gas-phase thermal degradation products of MGP LG305, (c) 3D TGA-FTIR spectrum of gas-phase thermal degradation products of MGP-T LG305.

The increased crosslinking significantly enhances the stability of the particles against swelling in organic solvents, ensuring that their spherical morphology is retained even after treatment with acetone (Fig. 6(f)). However, the dye tends to diffuse out of the particles when exposed to moderately polar solvents (Fig. S15) similar to the untempered particles. Under conditions relevant for optoelectronic or bio-related applications, where the microspheres are typically embedded in polymer matrices or dispersed in aqueous media, the dye remains stably incorporated in the particle structure.

For applications where the particles are exposed to solvents such as acetone or DCM, strategies to suppress dye diffusion could be considered. These include covalent attachment of the dye to the silsesquioxane framework, for example by using perylene-functionalized trialkoxysilane during the melting-gel synthesis,[64] or post-synthetic surface sealing through the

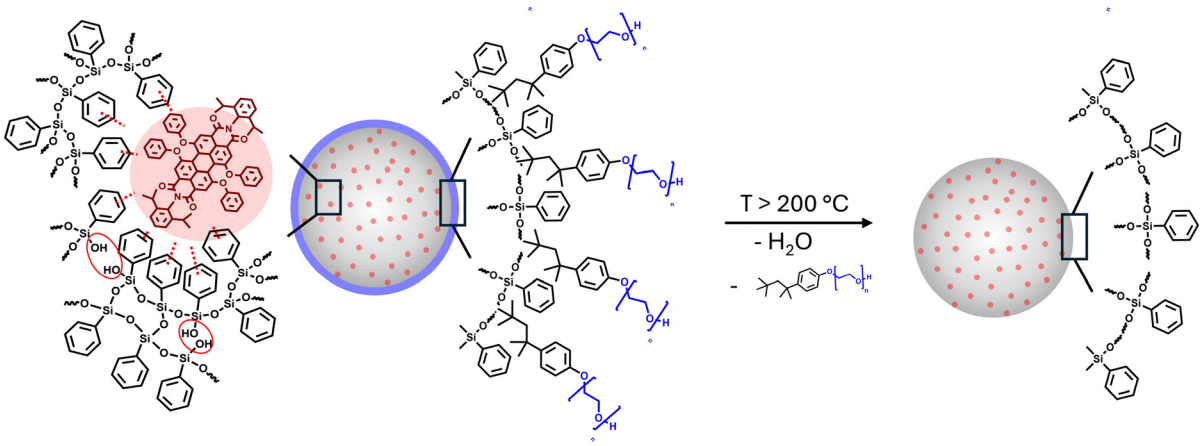

Fig. 8 Schematic representation of the influence of thermal treatment on MGP LG305. Perylene dye molecules are dispersed within the PPSQ matrix, while the surfactant resides on the particle surface. Upon heating to 200 °C, the degree of condensation increases and the surfactant is removed, changing the surface character from hydrophilic (surfactant-covered) to hydrophobic (phenyl-dominated).

addition of a dense silica shell or the application of thin polymeric coatings.[21,65]

The results indicate that additional thermal treatment effectively removes the surfactant from the particle surface (Fig. 8) and increases the degree of condensation, which enhances hydrophobicity and prevents dispersion in water.

Influence of stirring on particle size distribution

During microsphere synthesis, an emulsion is formed, and adjusting the stirring velocity with a standard laboratory stirring bar allows for controlled variations in microsphere size and size distribution. To optimize these parameters, five additional experiments were conducted, varying the stirring rate, duration, and method.

The stirring rate with a standard bar was adjusted from 500 (MGP-1) to 800 rpm (MGP-3), and the stirring time was increased from 1 h (MGP-1) to 2 h (MGP-2) at 500 rpm. To investigate the impact of high-energy processes on particle morphology, an ultrasonic finger (150 W, MGP-US) or an Ultra-Turrax™ disperser (10 000 rpm, MGP-UT) was applied after stirring at 500 rpm for 10 minutes. All experiments were performed using the hot emulsion of the precursor material MG LG305 before the addition of sodium hydroxide, which initiated consolidation and suspension formation, respectively.

The particle size and distribution were determined by measuring and counting particles from microscopy images (Fig. S17–S21). All measured particles fall within a small micrometer range, regardless of the procedure used. Stirring the emulsion at 500 rpm for 1 or 2 h (MGP-1/2) does not significantly alter the particle size distribution (Fig. 9). Increasing the stirring speed to 800 rpm (MGP-3) results in a narrower size distribution and smaller particle sizes. Additional ultrasonic treatment (MGP-US) leads to a broader distribution and larger particle sizes (MGP-US). The narrowest size distribution and the smallest particles were obtained using the Ultra-Turrax™ dispenser (MGP-UT).

Overall, when using a standard stirring bar, an increase of stirring velocity leads to a decrease in both particle size and size distribution. Increasing the stirring time at the same velocity does not lead to any significant change. In contrast to reports in the literature on sol–gel synthesis procedures,[66,67] the use of ultrasound does not reduce particle size but instead results in the broadest size distribution observed in this study. In general, the final droplet size is equal to the distribution immediately after droplet disruption by mechanical energy and is influenced by the dispersed phase viscosity.[68] The high viscosity prevents the destructions of the droplets by ultrasonic energy. Using the disperser results in smaller particles with a narrow distribution. This effect is attributed to the high rotational speed of the rotor, which generates intense shear and thrust forces, effectively breaking up the droplets. Consequently, mechanical energy is essential for producing smaller particles through droplet disruption, whereas the energy introduced by ultrasonic waves does not facilitate size reduction.

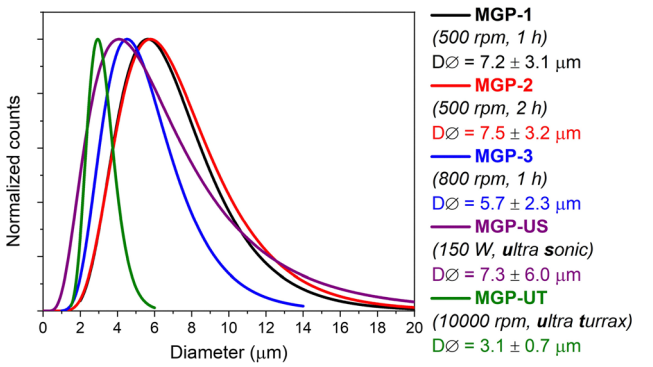

Fig. 9 Particle size distribution of the different experiments MGP-1, MGP-2, MGP-3 MGP-US and MGP-UT, determined by measuring and counting particles from microscopy images.

Photophysical properties of the dye microspheres

The perylene dye LG305 was incorporated into the precursor melting gel during gelation. Its high solubility in phenyl-containing matrices ensures homogeneous distribution.[36] Once embedded in the PPSQ network, dye aggregation is markedly reduced, as evidenced by the pronounced increase in the average fluorescence lifetime from 0.8 ns in the neat dye to 12.4 ns in MG LG305 (1150 ppm) (Fig. S22 and Table S3). This effect is attributed to the reduced chromophore mobility in the rigid matrix and may be further supported by weak π–π interactions between the perylene cores and the phenyl groups of the silsesquioxane, which can spatially separate chromophores and thereby suppress aggregation.[4,36]

The isolated and heat-treated microspheres exhibit red fluorescence, with two emission maxima at 622 nm and 647 nm (Fig. 10(a)). The excitation spectrum displays three bands at 578 nm, 530 nm and 440 nm. Compared to the fluorescence spectra of LG305 in toluene, a slight bathochromic shift in emission is observed (the Stokes shift, which was determined to be 29 nm in toluene, increases to 44 nm in the microspheres).[36] The absolute quantum yield of the microspheres was 64%, while in the precursor material MG LG305 the quantum yield is higher with 83%. A morphology and size-dependent decrease in quantum yield in silica and polymeric particles has already been reported.[69] The observed shift in emission and reduction in quantum yield are attributed to reabsorption processes within the sample, induced by spectral distortions caused by scattering and reabsorption effects. These effects arise due to the transition from transparent hybrid to a microparticle powder, altering the solid-phase morphology.[70,71]

Since the dye can be incorporated into the precursor gel in any quantity, the content of the hydrophobic component in the particles can be adjusted as needed. To demonstrate this, melting gels with varying dye concentrations (220 to 26 000 ppm, Fig. 10(b)) were prepared and used to synthesize microspheres. Particles with a dye concentration of 4350 ppm exhibited the highest quantum yield of 75%. At lower concentrations, the number of emitting centers is reduced, while at higher concentrations π–π stacking between perylene chromophores causes aggregation and fluorescence quenching, leading to a significant reduction in quantum yield.[72] The optimum at intermediate loading therefore reflects the balance between efficient excitation and the onset of concentration quenching, with the PPSQ matrix playing a decisive role in defining this

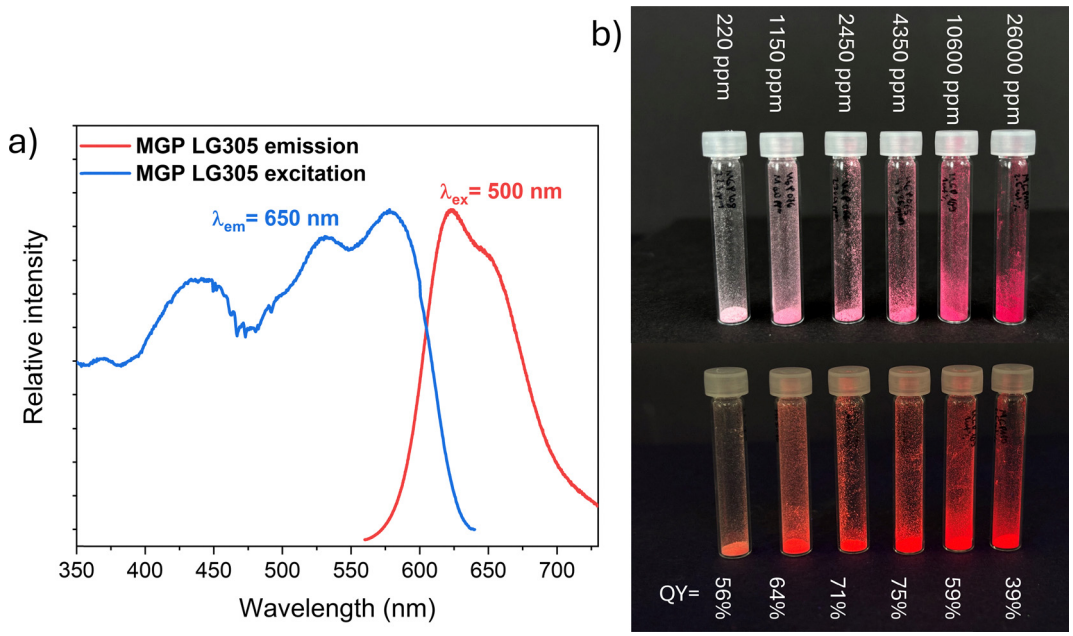

Fig. 10 (a) Emission and excitation spectra of MGP LG305 (1150 ppm LG305) at an excitation wavelength of 500 nm and an emission wavelength of 650 nm, (b) image of MGP LG305 with varying dye concentrations (220–26 000 ppm) under natural light (top) and 450 nm light (bottom), along with their respective quantum yields (QY).

regime by stabilizing isolated chromophores and delaying aggregation.[4,36,73]

Although aggregation-induced quenching cannot be fully avoided at high dye loadings, the integration of a hydrophobic perylene dye into PSSQ microspheres could be realized in a wide concentration range, yielding a fluorescent microsphere powder.

Physical incorporation of alternative dyes and encapsulation in a secondary encapsulation material

Due to the straightforward integration of dyes into the precursor gel, not only LG305 but also other dyes can be incorporated into the particles. It is essential that these molecules are stable under acidic and basic conditions and sufficiently hydrophobic to remain within the emulsion during synthesis without leaching. As an example, additional perylene-based dyes such as Oracet® FL Pink 285 and Oracet® FL Orange 240 were embedded in silica particles using the melt emulsion strategy (Fig. 11, further pictures and fluorescence spectra can be found in Fig. S23 and S24). All particles exhibited the characteristic excitation and emission of the incorporated molecules, confirming successful integration.

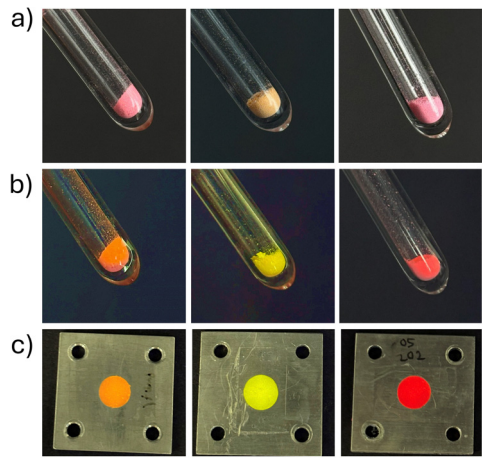

Fig. 11 Microspheres with encapsulated Oracet® FL Pink 285, Oracet® FL Orange 240, and Lumogen® F Red 305 (from left to right): (a) under natural light, (b) under 450 nm light, (c) integrated into polymethylphenylsiloxane resin cured in aluminum frames, under 450 nm light.

For applications such as organic hybrid LEDs or luminescent solar concentrators, the microspheres must be homogeneously encapsulated within a polymer matrix. Therefore, the temperature treated particles were integrated into an elastomeric two-component polyphenylmethylsiloxane resin (Dow Corning OE6630) which cures *via* a hydrosilylation reaction. The resulting composite materials exhibited a homogenous distribution of microspheres and characteristic fluorescence under UV light exposure (Fig. 11(c) and Fig. S25).

This experiment demonstrates that the microsphere synthesis *via* melt emulsion is not limited to LG305, but can also be extended to other hydrophobic dyes. It is conceivable that, beyond dyes, other hydrophobic molecules could be incorporated by the same approach. Owing to the good biocompatibility of the silsesquioxane matrix, this may also open opportunities for the encapsulation of drugs or fragrances, which is of interest in cosmetic and pharmaceutical formulations.[74,75]

Furthermore, this part highlights the potential use of the dye-loaded microspheres as bulk components in optical materials, for example in light-conversion applications.[4]

Conclusion

Acid-catalyzed hydrolysis and condensation of phenyltrimethoxysilane yielded a partially crosslinked PPSQ, known as melting gel, which softens above 70 °C and consolidates above 130 °C. Incorporation of the hydrophobic perylene dye Lumogen® F Red 305 during gelation resulted in a red-colored fluorescent precursor material.

For the first time, a hot emulsification approach of a thermoplastic PPSQ was used to produce spherical ORMOSIL particles. The softening of the precursor enabled emulsification in hot surfactant–water mixtures, followed by NaOH-catalyzed curing to rigid microspheres. Depending on the mechanical energy input during emulsion formation, different particle sizes and size distributions were achieved, with an optimized mean diameter of 3.1 ± 0.7 μm using an Ultra-Turrax disperser.

Spectroscopic analyses and PXRD measurements revealed that the PPSQ network consisted of partially crosslinked structures with predominantly ladder-like motifs. A surfactant layer of Triton™ X was detected on the particle surface. Additional heat treatment led to nearly complete crosslinking of the microsphere framework and the simultaneous surfactant removal, as confirmed by TGA, thereby converting the particle surface from hydrophilic (surfactant-covered) to hydrophobic (phenyl dominated).

Fluorescence lifetime measurements on the precursor gel showed a pronounced increase in lifetime upon dye encapsulation, while concentration-dependent quantum yield studies indicated enhanced emission within a defined concentration range. Microspheres with dye loadings between 220 and 26 000 ppm LG305 were prepared, with the maximum quantum yield of 75% observed at ~4350 ppm. The photophysical results suggest that the dye distributes homogeneously during synthesis due to its good solubility in the phenyl-rich hydrophobic matrix, while the aromatic groups of the host contribute to the effective separation of chromophores and reduced aggregation.

In aqueous solvents (water, ethanol), the dye remained stably encapsulated, whereas exposure to moderately polar organic solvents such as acetone or chloroform led to leaching.

Finally, other hydrophobic dyes such as Oracet® FL Pink 285 or Oracet® FL Orange 240, were successfully incorporated into microspheres *via* the melt-emulsion strategy. The fluorescent particles can then be incorporated into a secondary encapsulation material, with the siloxane-based particle matrix acting as a protective barrier against external influences, like moisture, oxygen or high temperatures.

Beyond optoelectronic and light-harvesting applications, this new approach also opens opportunities in cosmetics, for instance for the encapsulation of hydrophobic drugs or fragrances.

Declaration of AI and AI-assisted technologies in the writing process

During the preparation of this work, the authors utilized AI tools, including Deepl.com and ChatGPT to enhance the clarity of the language and to correct spelling, punctuation, and grammatical errors. After using these tools, the authors carefully reviewed and edited the content as necessary and take full responsibility for the accuracy and integrity of the publication.

Author contributions

Svenja Pohl: formal analysis, investigation, methodology, validation, visualization, writing – original draft. Nils Steinbrück: conceptualization, formal analysis, investigation, methodology, visualization, writing – original draft. Michał P. Pachnicz: investigation, writing – review & editing. Guido Kickelbick: conceptualization, funding acquisition, project administration, supervision, writing – review & editing.

Conflicts of interest

There are no conflicts to declare.

Data availability

The data supporting the findings of this study are available within the article and its supplementary information (SI). Supplementary information: NMR spectra, viscosity measurement, PXRD, TGA, leaching tests, SEM, microscopic images, fluorescence measurements, TCSPC analysis and additional photos. See DOI: **https://doi.org/10.1039/d5ma00849b**.

Acknowledgements

This research has been funded by the Federal Ministry of Education and Research (BMBF, Germany) in the project ORCA – Organic and rare earth reduced conversion materials for LED-based lightning (project number 03XP0050). Instrumentation and technical assistance for this work were provided by the Service Center X-ray Diffraction, with financial support from Saarland University and the German Science Foundation (project number INST 256/349-1). We would like to thank Elias Gießelmann for SP-MAS NMR support, Viktoria Kiefer for assistance with quantum yield and TCSPC experiments and BASF and Sunchemical for providing us with various fluorescent dyes.

References

1 W.-H. Zhang, X.-X. Hu and X.-B. Zhang, Dye-Doped Fluorescent Silica Nanoparticles for Live Cell and *In Vivo* Bioimaging, *Nanomaterials*, 2016, **6**, 81.
2 F. Gao, L. Tang, L. Dai and L. Wang, A fluorescence ratiometric nano-pH sensor based on dual-fluorophore-doped silica nanoparticles, *Spectrochim. Acta, Part A*, 2007, **67**, 517–521.
3 X. Huang, Z. P. Aguilar, H. Li, W. Lai, H. Wei, H. Xu and Y. Xiong, Fluorescent $Ru(phen)_3^{2+}$-Doped Silica Nanoparticles-Based ICTS Sensor for Quantitative Detection of Enrofloxacin Residues in Chicken Meat, *Anal. Chem.*, 2013, **85**, 5120–5128.

4 F. Corsini, E. Tatsi, A. Colombo, C. Dragonetti, C. Botta, S. Turri and G. Griffini, Highly emissive fluorescent silica-based core/shell nanoparticles for efficient and stable luminescent solar concentrators, *Nano Energy*, 2021, **80**, 105551.
5 S. Saita, K. Niwa, Y. B. Pottathara and H. Kawasaki, Highly bright full-color emission from dye-doped silica nanoparticles with prevention of dye self-quenching, *Opt. Mater.*, 2023, **139**, 113803.
6 X. Ning, J. Chittigori, Y. Li, G. Horner, Z. Zhou, C. K. Ullal and L. Schadler, Dye doped concentric shell nanoparticles for enhanced photophysical performance of downconverting light emitting diodes, *J. Colloid Interface Sci.*, 2019, **556**, 753–760.
7 S. Kwon, R. K. Singh, R. A. Perez, E. A. Abou Neel, H.-W. Kim and W. Chrzanowski, Silica-based mesoporous nanoparticles for controlled drug delivery, *J. Tissue Eng.*, 2013, **4**, 2041731413503357.
8 H. Li, X. Chen, D. Shen, F. Wu, R. Pleixats and J. Pan, Functionalized silica nanoparticles: classification, synthetic approaches and recent advances in adsorption applications, *Nanoscale*, 2021, **13**, 15998–16016.
9 Y. Choi, J. Kim, S. Yu and S. Hong, pH- and temperature-responsive radially porous silica nanoparticles with high-capacity drug loading for controlled drug delivery, *Nanotechnology*, 2020, **31**, 335103.
10 H.-S. Jung, Y.-J. Kim, S.-W. Ha and J.-K. Lee, White light-emitting diodes using thermally and photochemically stable fluorescent silica nanoparticles as color-converters, *J. Mater. Chem. C*, 2013, **1**, 5879–5884.
11 V. Gubala, G. Giovannini, F. Kunc, M. P. Monopoli and C. J. Moore, Dye-doped silica nanoparticles: synthesis, surface chemistry and bioapplications, *Cancer Nanotechnol.*, 2020, **11**, 1.
12 I. A. Rahman, P. Vejayakumaran, C. S. Sipaut, J. Ismail and C. K. Chee, Size-dependent physicochemical and optical properties of silica nanoparticles, *Mater. Chem. Phys.*, 2009, **114**, 328–332.
13 W. Stöber, A. Fink and E. Bohn, Controlled growth of monodisperse silica spheres in the micron size range, *J. Colloid Interface Sci.*, 1968, **26**, 62–69.
14 F. J. Arriagada and K. Osseo-Asare, Synthesis of Nanosize Silica in Aerosol OT Reverse Microemulsions, *J. Colloid Interface Sci.*, 1995, **170**, 8–17.
15 C. Odenwald and G. Kickelbick, Additive-free continuous synthesis of silica and ORMOSIL micro- and nanoparticles applying a microjet reactor, *J. Sol-Gel Sci. Technol.*, 2019, **89**, 343–353.
16 J. G. Croissant, X. Cattoën, J.-O. Durand, M. Wong Chi Man and N. M. Khashab, Organosilica hybrid nanomaterials with a high organic content: syntheses and applications of silsesquioxanes, *Nanoscale*, 2016, **8**, 19945–19972.
17 A. L. Mohamed, T. A. Khattab and A. G. Hassabo, Color-tunable encapsulated perylene-labeled silica fluorescent hybrid nanoparticles, *Results Chem.*, 2023, **5**, 100769.
18 X. Ren, B. Sun, C.-C. Tsai, Y. Tu, S. Leng, K. Li, Z. Kang, R. M. V. Horn, X. Li, M. Zhu, C. Wesdemiotis, W.-B. Zhang and S. Z. D. Cheng, Synthesis, Self-assembly, and Crystal Structure of a Shape-Persistent Polyhedral-Oligosilsesquioxane-Nanoparticle-Tethered Perylene Diimide, *J. Phys. Chem. B*, 2010, **114**, 4802–4810.
19 H.-J. Ben, Y. Fan, Y.-J. Shi, R. Liu, Y. Chen, X.-K. Ren and S. Jiang, Polyhedral-oligosilsesquioxane containing poly(methyl methacrylate) perylenebisimide microspheres with high solid state emission, *Dyes Pigm.*, 2017, **137**, 584–592.
20 J. Chen, S. Jia, X. Ji, M. Nourrein, H. Xiang, Z. Zhou, C.-L. Wang, B. Sun and M. Zhu, The morphologies and fluorescence quantum yields of perylene diimide dye-doped PS and PHVB microspheres, *RSC Adv.*, 2018, **8**, 35534–35538.
21 N. Klippel, G. Jung and G. Kickelbick, Hybrid inorganic-organic fluorescent silica nanoparticles - influence of dye binding modes on dye leaching, *J. Sol-Gel Sci. Technol.*, 2023, **107**, 2–19.
22 X. Lu, Y. Hou, J. Zha and Z. Xin, Facile Synthesis of Rhodamine B-Doped Poly(3-mercaptopropylsilsesquioxane) Fluorescent Microspheres with Controllable Size, *Ind. Eng. Chem. Res.*, 2013, **52**, 5880–5886.
23 C. L. Nistor, D. Donescu, R. Ianchis, C. Spataru, V. Raditoiu, C. Petcu, M. Ghiurea and C. Deleanu, Encapsulation of three different hydrophobic dyes in functionalized silica particles, *J. Sol-Gel Sci. Technol.*, 2011, **59**, 48–56.
24 R. Tapec, X. J. Zhao and W. Tan, Development of organic dye-doped silica nanoparticles for bioanalysis and biosensors, *Int. J. Nanosci.*, 2002, **2**, 405–409.
25 K. Köhler, A. Hensel, M. Kraut and H. P. Schuchmann, Melt emulsification—Is there a chance to produce particles without additives?, *Particuology*, 2011, **9**, 506–509.
26 W. Mehnert and K. Mäder, Solid lipid nanoparticles: Production, characterization and applications, *Adv. Drug Delivery Rev.*, 2012, **64**, 83–101.
27 S. Fanselow, S. E. Emamjomeh, K.-E. Wirth, J. Schmidt and W. Peukert, Production of spherical wax and polyolefin microparticles by melt emulsification for additive manufacturing, *Chem. Eng. Sci.*, 2016, **141**, 282–292.
28 L. C. Klein, S. Kallontzi, L. Fabris, A. Jitianu, C. Ryan, M. Aparicio, L. Lei and J. P. Singer, Applications of melting gels, *J. Sol-Gel Sci. Technol.*, 2019, **89**, 66–77.
29 L. C. Klein and A. Jitianu, Hybrid organic-inorganic gels that are melting gels, *J. Sol-Gel Sci. Technol.*, 2025, **113**, 30–38.
30 D. Yu, M. Kleemeier, G. M. Wu, B. Schartel, W. Q. Liu and A. Hartwig, A low melting organic-inorganic glass and its effect on flame retardancy of clay/epoxy composites, *Polymer*, 2011, **52**, 2120–2131.
31 A. Jitianu, J. Doyle, G. Amatucci and L. C. Klein, presented in part at the Proceeding at Material Science & Technology Pittsburgh, PA, 2008.
32 K. Kajihara, R. Suzuki, R. Seto, H. Itakura and M. Ishijima, Poly(cyclohexylsilsesquioxane)-Based Hydrophilic Thermoset-Resistant Deep-Ultraviolet-Transparent Glasses with Low Melting Temperatures, *ACS Appl. Mater. Interfaces*, 2023, **15**, 31880–31887.
33 B. Menaa, M. Takahashi, Y. Tokuda and T. Yoko, Preparation and properties of polyphenylsiloxane-based hybrid

glass films obtained from a non-aqueous coating sol via a single-step dip-coating, *Opt. Mater.*, 2007, **29**, 806–813.
34 S. Castelletto and A. Boretti, Luminescence solar concentrators: A technology update, *Nano Energy*, 2023, **109**, 108269.
35 N. Steinbrück and G. Kickelbick, Perylene polyphenylmethylsiloxanes for optoelectronic applications, *J. Polym. Sci., Part B: Polym. Phys.*, 2019, **57**, 1062–1073.
36 N. Steinbrück, M. Könemann and G. Kickelbick, Effect of polysiloxane encapsulation material compositions on emission behaviour and stabilities of perylene dyes, *RSC Adv.*, 2018, **8**, 18128–18138.
37 MestReNova, v14.2.0-26256, Mestrelab Research, S.L., Santiago de Compostela, Spain.
38 C. A. Schneider, W. S. Rasband and K. W. Eliceiri, NIH Image to ImageJ: 25 years of image analysis, *Nat. Methods*, 2012, **9**, 671–675.
39 *SymPhoTime, version 2.1.3764*, Pico-Quant, Berlin, Germany.
40 Topas 5, Bruker AXS, Karlsruhe, Germany.
41 S. Pohl, O. Janka, E. Füglein and G. Kickelbick, Thermoplastic Silsesquioxane Hybrid Polymers with a Local Ladder-Type Structure, *Macromolecules*, 2021, **54**, 3873–3885.
42 A. Jitianu, G. Amatucci and L. C. Klein, Phenyl-Substituted Siloxane Hybrid Gels that Soften Below 140 °C, *J. Am. Ceram. Soc.*, 2009, **92**, 36–40.
43 Y.-S. Li, Y. Wang and S. Ceesay, Vibrational spectra of phenyltriethoxysilane, phenyltrimethoxysilane and their sol–gels, *Spectrochim. Acta, Part A*, 2009, **71**, 1819–1824.
44 A. Jitianu, G. Gonzalez and L. C. Klein, Hybrid Sol–Gel Glasses with Glass-Transition Temperatures Below Room Temperature, *J. Am. Ceram. Soc.*, 2015, **98**, 3673–3679.
45 N. Hu, Y. Rao, S. Sun, L. Hou, P. Wu, S. Fan and B. Ye, Structural Evolution of Silica Gel and Silsesquioxane Using Thermal Curing, *Appl. Spectrosc.*, 2016, **70**, 1328–1338.
46 Z. Li, S. Tolbert and D. A. Loy, Hybrid Organic-Inorganic Membranes on Porous Supports by Size Exclusion and Thermal Sintering of Fluorescent Polyphenylsilsesquioxane Nanoparticles, *Macromol. Mater. Eng.*, 2013, **298** 715–721.
47 K. Katagiri, K. Hasegawa, A. Matsuda, M. Tatsumisago and T. Minami, Preparation of Transparent Thick Films by Electrophoretic Sol–Gel Deposition Using Phenyltriethoxysilane-Derived Particles, *J. Am. Ceram. Soc.*, 1998, **81**, 2501–2503.
48 R. H. Baney, M. Itoh, A. Sakakibara and T. Suzuki, Silsesquioxanes, *Chem. Rev.*, 1995, **95**, 1409–1430.
49 S. L. B. Lana and A. B. Seddon, X-Ray Diffraction Studies of Sol–Gel Derived ORMOSILs Based on Combinations of Tetramethoxysilane and Trimethoxysilane, *J. Sol-Gel Sci. Technol.*, 1998, **13**, 461–466.
50 S.-S. Choi, A. S. Lee, S. S. Hwang and K.-Y. Baek, Structural Control of Fully Condensed Polysilsesquioxanes: Ladderlike vs Cage Structured Polyphenylsilsesquioxanes, *Macromolecules*, 2015, **48**, 6063–6070.
51 K. A. Andrianov, A. A. Zhdanov and V. Y. Levin, Some Physical Properties of Organosilicon Ladder Polymers, *Annu. Rev. Mater. Res.*, 1978, **8**, 313–326.
52 Z. Xinsheng, S. Lianghe and H. Chaoran, More on the Structures of Polyphenylsilsesquioxanes, *Chin. J. Polym. Sci.*, 1987, **5**, 353–358.
53 L. A. S. D. A. Prado, E. Radovanovic, H. O. Pastore, I. V. P. Yoshida and I. L. Torriani, Poly(phenylsilsesquioxane)s: Structural and morphological characterization, *J. Polym. Sci., Part A: Polym. Chem.*, 2000, **38**, 1580–1589.
54 I. M. Petrova, A. K. Buryak, A. S. Peregudov, T. V. Strelkova, E. G. Kononova, I. S. Bushmarinov and N. N. Makarova, Effect of stereoisomerism of (tetrahydroxy)(tetraphenyl)cyclotetrasiloxanes on the siloxane framework in polyphenylsilsesquioxanes obtained by polycondensation in the presence of layered-architecture compounds, *Mendeleev Commun.*, 2015, **25**, 229–231.
55 E. S. Park, H. W. Ro, C. V. Nguyen, R. L. Jaffe and D. Y. Yoon, Infrared Spectroscopy Study of Microstructures of Poly(silsesquioxane)s, *Chem. Mater.*, 2008, **20**, 1548–1554.
56 A. A. Anisimov, N. V. Polshchikova, Y. S. Vysochinskaya, P. A. Zader, G. G. Nikiforova, A. S. Peregudov, M. I. Buzin, O. I. Shchegolikhina and A. M. Muzafarov, Condensation of all-*cis*-tetraphenylcyclotetrasiloxanetetraol in ammonia: new method for preparation of ladder-like polyphenylsilsesquioxanes, *Mendeleev Commun.*, 2019, **29**, 421–423.
57 W. Zhang, X. Wang, Y. Wu, Z. Qi and R. Yang, Preparation and Characterization of Organic-Inorganic Hybrid Macrocyclic Compounds: Cyclic Ladder-like Polyphenylsilsesquioxanes, *Inorg. Chem.*, 2018, **57**, 3883–3892.
58 J.-F. Kannengießer, B. Morgenstern, O. Janka and G. Kickelbick, Oligo-Condensation Reactions of Silanediols with Conservation of Solid-State-Structural Features, *Chem. – Eur. J.*, 2024, **30**, e202303343.
59 C. J. Brinker, Hydrolysis and condensation of silicates: Effects on structure, *J. Non-Cryst. Solids*, 1988, **100**, 31–50.
60 K. Mitsuda, H. Kimura and T. Murahashi, Evaporation and decomposition of Triton X-100 under various gases and temperatures, *J. Mater. Sci.*, 1989, **24**, 413–419.
61 H. Masai, M. Takahashi, Y. Tokuda and T. Yoko, Enhancement of Polycondensation Reaction by Diethyl Ether-Aqueous NaOH Immiscible Two Phase Liquid Treatment of Phenyl-Modified Polysiloxane Glass, *J. Ceram. Soc. Jpn.*, 2005, **113**, 259–262.
62 D. Schneider, D. Loy, B. Baugher, D. Wheeler, R. Assink, T. Alam and R. Saunders, Preparation and characterization of phenyl-, benzyl-, and phenethyl-substituted polysilsesquioxanes, *Polym. Prepr.*, 1998, **39**, 513–514.
63 M. Nowacka, A. Kowalewska and T. Makowski, Structural studies on ladder phenylsilsesquioxane oligomers formed by polycondensation of cyclotetrasiloxanetetraols, *Polymer*, 2016, **87**, 81–89.
64 D. Sriramulu, S. P. Turaga, A. A. Bettiol and S. Valiyaveettil, Molecular Organization Induced Anisotropic Properties of Perylene – Silica Hybrid Nanoparticles, *Sci. Rep.*, 2017, **7**, 7842.
65 H. Ow, D. R. Larson, M. Srivastava, B. A. Baird, W. W. Webb and U. Wiesner, Bright and Stable Core−Shell Fluorescent Silica Nanoparticles, *Nano Lett.*, 2005, **5**, 113–117.

66 K. A. Mani, N. Yaakov, Y. Itzhaik Alkotzer, E. Zelikman and G. Mechrez, A Robust Fabrication Method for Amphiphilic Janus Particles via Immobilization on Polycarbonate Microspheres, *Polymers*, 2018, **10**, 900.

67 H. E. Romeo, M. A. Fanovich, R. J. J. Williams, L. Matějka, J. Pleštil and J. Brus, Fast Synthesis of Nanostructured Microspheres of a Bridged Silsesquioxane via Ultrasound-Assisted Sol–Gel Processing, *Macromol. Chem. Phys.*, 2008, **210**, 172–178.

68 O. Behrend, K. Ax and H. Schubert, Influence of continuous phase viscosity on emulsification by ultrasound, *Ultrason. Sonochem.*, 2000, **7**, 77–85.

69 K. Trofymchuk, A. Reisch, I. Shulov, Y. Mély and A. S. Klymchenko, Tuning the color and photostability of perylene diimides inside polymer nanoparticles: towards biodegradable substitutes of quantum dots, *Nanoscale*, 2014, **6**, 12934–12942.

70 L. R. Wilson and B. S. Richards, Measurement method for photoluminescent quantum yields of fluorescent organic dyes in polymethyl methacrylate for luminescent solar concentrators, *Appl. Opt.*, 2009, **48**, 212–220.

71 M. G. Lagorio and E. San Román, How Does Light Scattering Affect Luminescence? Fluorescence Spectra and Quantum Yields in the Solid Phase, *J. Chem. Educ.*, 2002, **79**, 1362–1367.

72 E. Lucenti, C. Botta, E. Cariati, S. Righetto, M. Scarpellini, E. Tordin and R. Ugo, New organic–inorganic hybrid materials based on perylene diimide–polyhedral oligomeric silsesquioxane dyes with reduced quenching of the emission in the solid state, *Dyes Pigm.*, 2013, **96**, 748–755.

73 M. Buffa, S. Carturan, M. G. Debije, A. Quaranta and G. Maggioni, Dye-doped polysiloxane rubbers for luminescent solar concentrator systems, *Sol. Energy Mater. Sol. Cells*, 2012, **103**, 114–118.

74 L. J. Green, N. D. Bhatia, O. Toledano, M. Erlich, A. Spizuoco, B. C. Goodyear, J. P. York and J. Jakus, Silica-based microencapsulation used in topical dermatologic applications, *Arch. Dermatol. Res.*, 2023, **315**, 2787–2793.

75 J. Yeom, W. S. Shim and N. G. Kang, Eco-Friendly Silica Microcapsules with Improved Fragrance Retention, *Appl. Sci.*, 2022, **12**, 6759.